Following Ostwald ripening in nanoalloys by high-resolution imaging with single-atom chemical sensitivity

D. Alloyeau, T. Oikawa, J. Nelayah, G. Wang, and C. Ricolleau

Related Articles

Effect of Mg interlayer on perpendicular magnetic anisotropy of CoFeB films in MgO/Mg/CoFeB/Ta structure
Appl. Phys. Lett. 101, 122414 (2012)

Propagation of light in serially coupled plasmonic nanowire dimer: Geometry dependence and polarization control
Appl. Phys. Lett. 101, 111111 (2012)

Quantitative evaluation of hidden defects in cast iron components using ultrasound activated lock-in vibrothermography
Rev. Sci. Instrum. 83, 094902 (2012)

The microstructure network and thermoelectric properties of bulk (Bi,Sb)2Te3
Appl. Phys. Lett. 101, 113902 (2012)

Magnetostriction and ΔE effect of melt-spun (Fe81−xCoxGa19)80B20 ribbons
J. Appl. Phys. 112, 053904 (2012)

Additional information on Appl. Phys. Lett.

Journal Homepage: http://apl.aip.org/

Journal Information: http://apl.aip.org/about/about_the_journal

Top downloads: http://apl.aip.org/features/most_downloaded

Information for Authors: http://apl.aip.org/authors

Following Ostwald ripening in nanoalloys by high-resolution imaging with single-atom chemical sensitivity

D. Alloyeau,[1,a)] T. Oikawa,[1,2] J. Nelayah,[1] G. Wang,[1] and C. Ricolleau[1]

[1]*Laboratoire Matériaux et Phénomènes Quantiques, Université Paris Diderot/CNRS, UMR 7162, Bâtiment Condorcet, 4 rue Elsa Morante, 75205 Paris Cedex 13, France*
[2]*JEOL Ltd, 1-2 Musashino 3-Chome, Akishima, Tokyo 196-8558, Japan*

Several studies have shown that substantial compositional changes can occur during the coarsening of bimetallic nanoparticles (CoPt, AuPd). To explain this phenomenon that could dramatically impacts all the technologically relevant properties of nanoalloys, we have exploited the sensitivity of the latest generation of electron microscope to prove that during the beam-induced coarsening of CoPt nanoparticles, the dynamic of atom exchanges between the particles is different for Co and Pt. By distinguishing the chemical nature of individual atoms of Co and Pt, while they are diffusing on a carbon film, we have clearly shown that Co atoms have a higher mobility than Pt atoms because of their higher evaporation rate from the particles. These atomic-scale observations bring the experimental evidence on the origin of the compositional changes in nanoalloys induced by Ostwald ripening mechanisms. © *2012 American Institute of Physics*. [http://dx.doi.org/10.1063/1.4754111]

Ostwald ripening plays a determinant role in the evolution of cluster size during both chemical and physical synthesis of nanoparticles (NPs). This thermoactivated process was firstly described by the Lifshitz-Slyozov-Wagner theory.[1,2] When they receive energy in form of heat, larger particles are more energetically favored than smaller particles. Consequently, smaller clusters dissolve and the evaporated atoms redeposit on the surfaces of larger particles. However, this phenomenon becomes more complex when considering the coarsening of multi-element NPs. Recently, some attention has been paid to the impact of this phenomenon on the composition of bimetallic NPs,[3–5] so called nanoalloys. Substantial compositional changes during high temperature annealing have been observed in CoPt[3] and AuPd[4] NPs. In these nanosystems, the larger particles formed by the growth mechanisms present a large excess of Co (or Pd) after annealing. It has recently been suggested that the compositional change measured in CoPt NPs occurs during Oswald ripening process and originates from the higher evaporation rate of Co atoms from the NPs.[3] The unique potential of nanoalloys arises from the fact that their physical or chemical properties can be tuned by varying their composition, as well as their size and morphology.[6] Therefore, understanding the Ostwald ripening mechanisms in multi-element NPs is of primary importance to control their many technologically relevant properties.

Here, aberration-corrected high resolution transmission electron microscopy (HRTEM) was exploited to provide the experimental evidence that during the beam-induced coarsening of CoPt NPs, the exchange of atoms between the NPs is more important for Co than for Pt. Therefore, this single atom quantitative analysis sheds unambiguous light on the cause of the compositional changes induced by the Ostwald ripening mechanisms in multi-element NPs.

Co, Pt, and $Co_{50}Pt_{50}$ NPs thin films were separately produced by pulsed laser deposition in a high vacuum chamber ($<10^{-7}$ mbar). This vapor phase deposition technique,[7–10] was used to deposit cobalt and platinum by using a KrF excimer laser at 248 nm with a pulse duration of 25 ns at a repetition rate of 5 Hz. A free standing very thin amorphous carbon film deposited on a commercial TEM lacey grid was used as the substrate. The thickness of the carbon film (5 nm) was precisely measured before vapor phase deposition, by using both the electron energy loss spectroscopy (EELS) log-ratio method[11] and a home-made technique.[12] Following the synthesis, the specimens were immediately transferred into the TEM to avoid contamination and air oxidation. Quantitative HRTEM analyses of single diffusing atoms were performed by using the JEM-ARM200F microscope. The unique configuration of this microscope[13] is perfectly adapted to the fascinating study of single atom diffusion. Indeed, the combination of the JEOL cold field emission gun (FEG)[14] and the CEOS corrector[15] to compensate the spherical aberration of the objective lens, associated to the enhanced mechanical and electrical stabilities of the JEM-ARM200F microscope, allows reaching a point resolution of 75 pm at 200 kV.[13] More importantly, the high brightness of the cold FEG substantially improved imaging sensitivity that is essential for quantitative high resolution imaging and the study of single atoms.

Single atoms are the most basic weak phase objects in electron microscopy. Therefore, the interaction between the electron wave and an atom only induces a phase shift with negligible amplitude variation in the resulting electron wave. This leads to weak single-atom contrast that depends strongly on the scattering potential of the atom (Z number) and the optical parameters of the microscope. Although single atom imaging by HRTEM has been demonstrated for a few decades,[16,17] the performance of the latest generation TEM allows now the observation of individual atoms in a wide range of materials.[18–21] In the present experiment, the coarsening of CoPt NPs supported by a very thin carbon film

---

a)Author to whom correspondence should be addressed. Electronic mail: damien.alloyeau@univ-paris-diderot.fr.
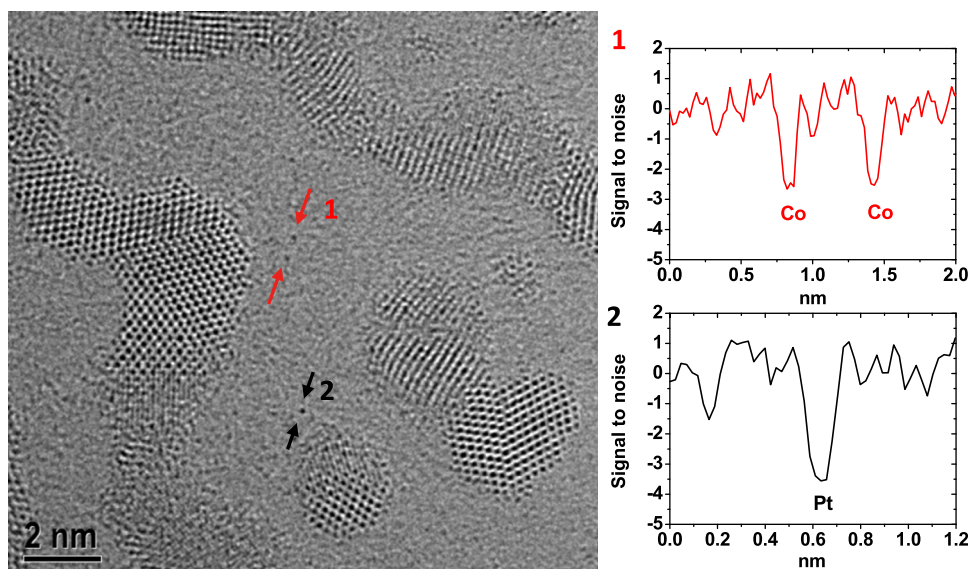
FIG. 1. (a) HRTEM images of CoPt nanoparticles. Individual Co and Pt atoms appear as additional black contrast on the carbon substrate (see Video 1). The two SNR profiles (right side of the figure) were measured between the two corresponding arrows in the TEM images. The SNR profile 1 shows two Co atoms (SNR of −2.6), whereas the SNR profile 2 shows a Pt atom (SNR of −3.5) (enhanced online) Video 1 [URL: http://dx.doi.org/10.1063/1.4754111.1].

is activated by the 200 kV electron beam. Many TEM observations of metallic NPs have reported that the two main growth mechanisms, coalescence and Ostwald ripening, can be activated by highly accelerated electrons.[22–24] For maintaining the energy transferred to the particles constant, all the following TEM experiments were performed by using the same electron dose (6.5×10^5 e$^-$/nm^2). As illustrated in Figure 1, individual metal atoms appear as additional contrast in the carbon film between the NPs. However, these contrasts appear and disappear from frame to frame when image series are recorded with a 0.2 s time interval. This direct observation of single-atom dynamic between bimetallic NPs shows that the diffusion of metallic atoms on carbon substrate, on which migration barriers around 0.1 eV were reported,[25] is too fast to follow the path of a single atom from a particle to another. However, the diffusing atoms are trapped long enough in energetically favorable sites of the carbon film to be observed on HRTEM images.

In this letter, we focus on distinguishing the chemical nature of the diffusing atoms (Co or Pt) to compare the kinetic of Ostwald ripening for Co and Pt. However, the interpretation of HRTEM contrasts requires the comparison of experimental and simulated images. HRTEM images were simulated with JEMS software,[26] by using the aberration coefficients experimentally calculated by the CEOS corrector software. The tuning of the aberration corrector was frequently performed during our HRTEM experiments in order to minimize the impact of the aberration coefficient fluctuations over time.[27] The atomic model used for these simulations consist in a 2 nm CoPt NPs as well as one Co and one Pt atom on a 5 nm-thick carbon film (Figure 2(a)). The atomic potential of this model was calculated by using the Weickenmeier-Kohl form factors.[28] We used the signal to noise ratio (SNR) definition proposed by Rose[29] to quantify the simulated and experimental contrast of single atoms in the images. The signal is defined as the incremental change in the image intensity due to the atoms and the noise is the standard deviation of the carbon film intensity. The SNR of Co and Pt single atoms is reported as a function of focus in Figure 2(b). Image simulations predict that the chemical analysis of single atom can best be achieved in a focus window from −2 to −10 nm, in which the SNR is flat against the focal distance and the contrast difference between Co and Pt is substantial (from −2 and −2.6 for Co and from −3
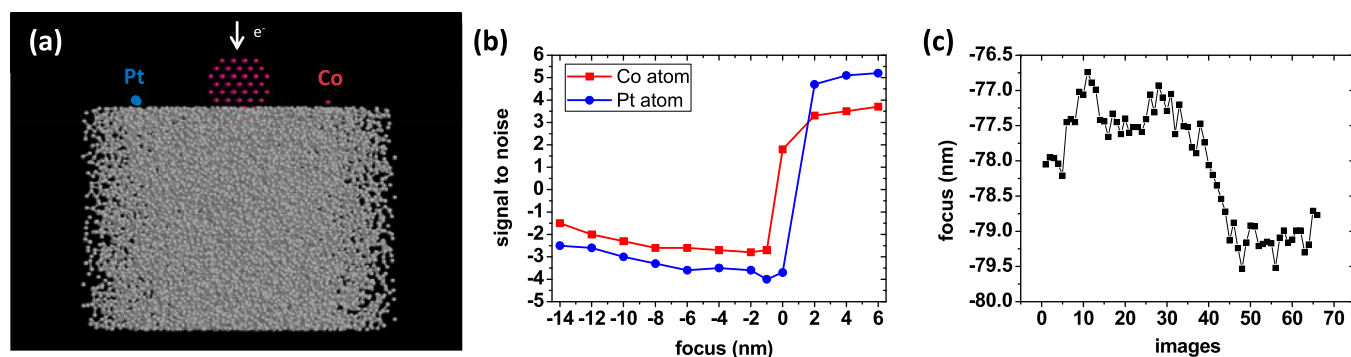

FIG. 2. (a) Atomic model used for HRTEM image simulations. The 5 nm-thick carbon film consists in a random arrangement of carbon atoms with atomic distance of 0.142 nm and a film density of 2.2 g/cm^2. The white arrow indicates the electron pathway. (b) SNR of the Co (red squares) and Pt (bleu circles) atom measured on the simulated images as a function of the focal distance of the objective lens. The aberration coefficients experimentally calculated by the CEOS corrector software were used for the simulation (two-fold astigmatism <1 nm, three-fold astigmatism = 36 nm, axial coma = 11 nm, and spherical aberration coefficient = 2 μm). (c) Focus stability experimentally measured on an image series of a carbon film recorded with a 2 s time interval. The focal distance was automatically calculated by the corrector software, by using the Thon rings on the fast Fourier transform of each image. The focus instability is mainly due to carbon film oscillations.

to −3.6 for Pt). Figure 2(c) shows the focus stability experimentally measured on a carbon film. Over two minutes, the focal distance varies in a range of 2.7 nm because of carbon film oscillations. Thus, all the experimental images were acquired in the focus window from −2 to −10 nm, by using the Thon rings to determine the experimental focal distance. Since this focus window is larger than the focal distance instability, this protocol allows acquiring image series over several minutes, on which the attenuation of the incoming electron beam due to a single atom (i.e., black contrast) will always be higher for Pt than Co.

As an experimental calibration, these single atom contrast analyses were firstly performed on pure Co and pure Pt NPs. We observe on the histograms plotted in Figure 3 that the SNR of single atoms measured on these two samples follows a Gaussian distribution. In good agreement with image simulations, these Gaussian profiles are centred on −2.68 for Co atoms and −3.18 for Pt atoms, with a standard deviation of 0.18 and 0.30, respectively. These results show that the sensitivity of the microscope enhanced by the high brightness of the cold FEG and the reinforced mechanical stability of the ARM 200F, allows distinguishing the chemical nature of individual atoms of Co and Pt, while they are diffusing on a carbon film. We note that quantitative agreement between experimental and simulated single atom contrast can be improved by accounting for the modulation transfer function (MTF) of the CCD camera.[18,30] Here, the MTF was not taken into account, but we always used the same magnification (×800 000) in order to have the same MTF effects in all the HRTEM images.

As illustrated on Figure 1, both Co and Pt atoms were detected during the coarsening of CoPt NPs. Indeed, the first intensity profile reveals the presence of two Co atoms on the carbon film, (SNR of −2.6) whereas the second intensity profile shows a Pt atom (SNR of −3.5). Therefore, with these illumination conditions, the energy transferred to the CoPt NPs allows overcoming the energy barrier for atomic evaporation from a NP to the substrate either for Co or Pt atoms. However, the statistical analysis realised by measuring the SNR of 100 single atoms clearly shows that the kinetic of atomic exchange is faster for Co than Pt. The histograms of Figure 3(c) presents the two Gaussian peaks characteristic for Pt (centred on −3.24 with a standard deviation of 0.26) and Co (centred on −2.52 with a standard deviation of 0.32) signals, but the amplitude of the Gaussian distributions for Co is twice as high as the one for Pt. In fact, among the 100 analysed atoms, 59 are Co, 32 are Pt, and 7 are undetermined.

Thermodynamic considerations explicitly demonstrate that Ostwald ripening is first limited by the evaporation rate of atoms from the NPs rather than by surface diffusion. Indeed, for evaporation to the substrate, the energy barrier ΔE is at least given by the energy difference between initial and final states. In a first approximation, neglecting cluster size effects, this leads to $\Delta E \geq E_a - E_c$, where E_a is the adsorption energy of an adatom on the surface and E_c is the bulk cohesive energy of the metal. E_c^{Co} and E_c^{Pt} are −4.386 eV and −5.853 eV, respectively.[31] The adsorption energy of Co and Pt atoms on graphene has been obtained by *ab initio* calculation.[32,33] They can be used as a first estimate of the adsorption energy of atoms on amorphous carbon ($E_a^{Co} = -1.3$ eV, and $E_a^{Pt} = -1.2$ eV). The energy barrier for atomic evaporation from a particle to the substrate is thus higher for Pt ($\Delta E^{Pt} \geq 4.7$ eV) than for Co ($\Delta E^{Co} \geq 3.1$ eV), and more than 30 times higher than the diffusion barriers of metallic atoms on carbon substrate.[25] This energetic reasoning shows that the mobility of Pt atoms during Oswald ripening is actually slowed down by their high desorption energy and not by the diffusion processes. This thermodynamic phenomenon induces both the faster kinetic of atomic exchange for Co atoms highlighted here by high resolution TEM, and the large excess of Co measured in the particles enlarged by Oswald ripening.[3]

The dynamical behaviour of very small NPs under beam irradiation observed at atomic resolution in Figure 4 confirms this theoretical interpretation. All these images were acquired in the focus window from −2 to −10 nm, in which atom columns of 2 nm cluster appear as black contrast. Figures 4(a)–4(d) show that the number of atom columns within a 2 nm Co NPs decrease very rapidly from 40 to 0 in a few seconds. On the contrary, with the same electron dose, 2 nm CoPt NPs (Figs. 4(e)–4(h)) and 2 nm Pt NPs[12] never dissolved. In spite of an important diffusion at the surface of the clusters, the number of atom columns within the NPs remains almost constant for several minutes. These results demonstrate that Pt atoms are a source of cohesion for small CoPt NPs, which explains their lower mobility than Co atoms during Ostwald ripening process.

To finish, when reducing the electron dose from 6.5×10^5 e⁻/nm² to 6.5×10^4 e⁻/nm², although the noise level of the images would not prevent the detection of single metal atoms, no atomic mobility is observed between the NPs.[12] These reduced-dose HRTEM conditions, in which the electron beam does not activate the growth mechanisms, give the opportunity to study thermally induced Ostwald
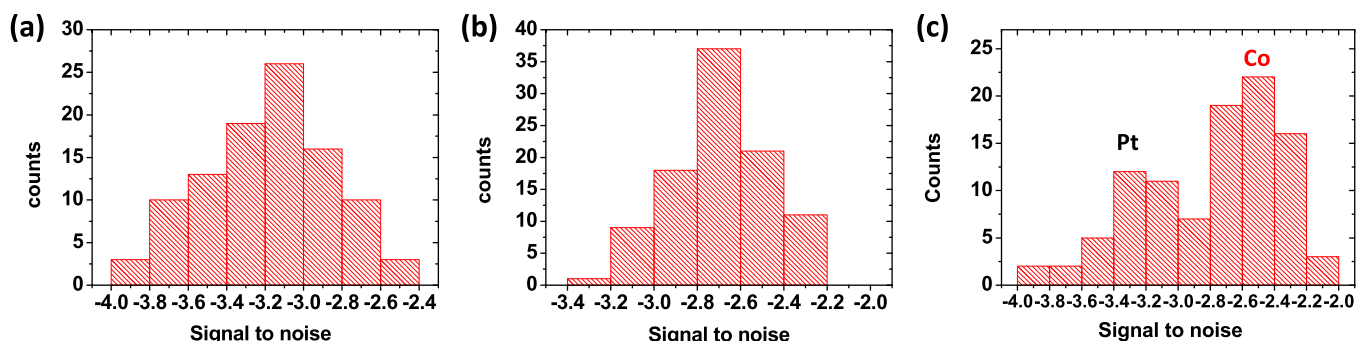

FIG. 3. Histogram of the single atom SNR experimentally measured between (a) pure Pt NPs and (b) pure Co NPs. (c) CoPt nanoparticles, the two Gaussian peaks centered at −3.24 and −2.52 correspond to the signal of Pt and Co, respectively.
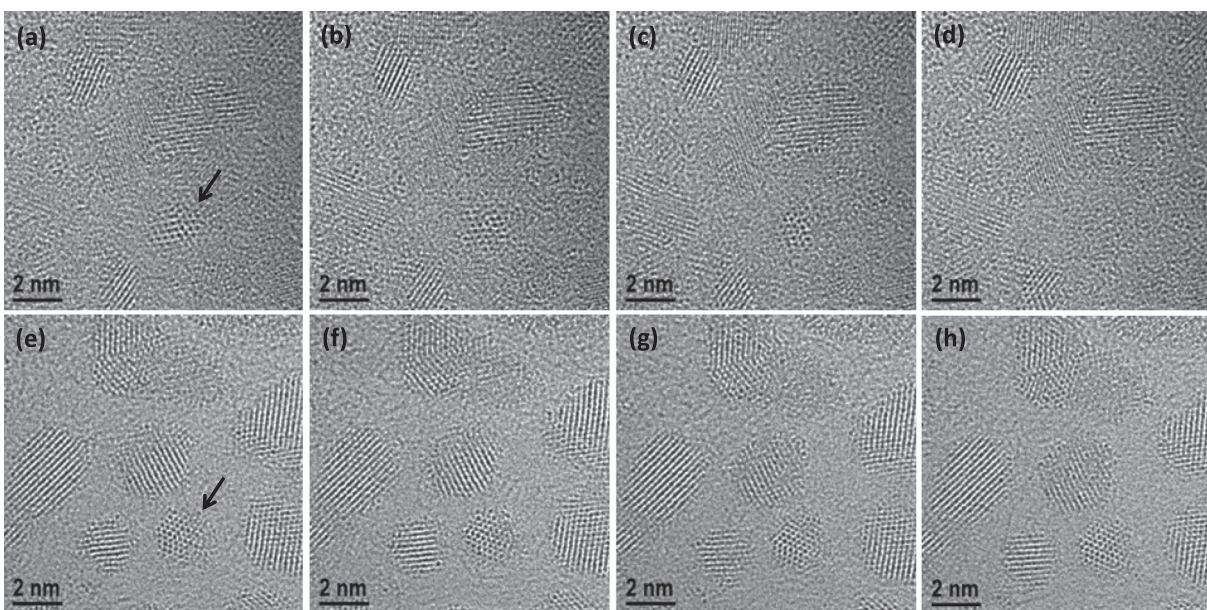
FIG. 4. Dynamical behaviour of very small NPs under electron beam irradiation observed at atomic resolution. (a) to (d) Pure Co NPs observed during 4 s. The black arrow in the first image (a) indicates a 2 nm Co NPs that is rapidly shrinking and completely disappears in the last image (d) (see Video 2). (e) to (h) CoPt NPs observed during 10 s. The black arrow in the first image (d) indicates a 2 nm CoPt NPs that is stable and maintains its cohesion (see Video 3) (enhanced online) Video 2 [URL: http://dx.doi.org/10.1063/1.4754111.2]; Video 3 [URL: http://dx.doi.org/10.1063/1.4754111.3].

ripening mechanisms at the atomic scale, by using a stability-enhanced *in situ* heating holder.[34]

We exploited the sensitivity of the latest generation of electron microscope to follow the dynamic of single atom exchanges between CoPt NPs during coarsening phenomena. By distinguishing the chemical nature of individual atoms of Co and Pt, while they are diffusing on a carbon film, we have shown that Co atoms have a higher mobility than Pt atoms because of their higher evaporation rate from the NPs. This result provides a concrete explanation for the compositional changes induced by the Ostwald ripening mechanisms in multi-element NPs.[3] More generally, our investigations highlight the performance of aberration-corrected HRTEM to extract quantitative information from dynamical process with single atom sensitivity, which can provide better insights into the characterization of crystal growth or catalytic reactions.

[1] I. M. Lifshitz and V. V. Slyozov, J. Phys. Chem. Solids **19**, 35 (1961).

[2] C. Wagner, Z. Elektrochem. **65**, 581 (1961).

[3] D. Alloyeau, G. Prévot, Y. Le Bouar, T. Oikawa, C. Langlois, A. Loiseau, and C. Ricolleau, Phys. Rev. Lett. **105**, 255901 (2010).

[4] M. Di Vece, S. Bals, J. Verbeeck, P. Lievens, and G. Van Tendeloo, Phys. Rev. B **80**, 125420 (2009).

[5] A. A. Herzing, M. Watanabe, J. K. Edwards, M. Conte, Z.-R. Tang, G. J. Hutchings, and C. J. Kiely, Faraday Discuss. **138**, 337 (2008).

[6] D. Alloyeau, C. Mottet, and C. Ricolleau, *Nanoalloys: Synthesis, Structure and Properties* (Springer-Verlag, London, 2012).

[7] D. Alloyeau, C. Langlois, C. Ricolleau, Y. Le Bouar, and A. Loiseau, Nanotechnology **18**, 375301 (2007).

[8] D. Alloyeau, C. Ricolleau, C. Langlois, Y. Le Bouar, and A. Loiseau, Beilstein J. Nanotechnol. **1**, 55 (2010).

[9] D. Alloyeau, C. Ricolleau, T. Oikawa, C. Langlois, Y. Le Bouar, and A. Loiseau, Ultramicroscopy **108**, 656 (2008).

[10] D. Alloyeau, C. Ricolleau, T. Oikawa, C. Langlois, Y. Le Bouar, and A. Loiseau, Ultramicroscopy **109**, 788 (2009).

[11] R. F. Egerton, *Electron Energy-Loss Spectroscopy in Electron Microscope* (Plemium, New York, 1996), p. 301.

[12] See supplementary material at http://dx.doi.org/10.1063/1.4754111 for the film thickness measurement methods, the time series HRTEM experiments on a 2 nm Pt NPs, and the dose-reduced HRTEM analyses.

[13] C. Ricolleau, J. Nelayah, T. Oikawa, Y. Kohno, N. Braidy, G. Wang, F. Hue, and D. Alloyeau, JEOL News **47**, 2 (2012).

[14] Y. Kohno, E. Okunishi, T. Tomita, I. Ishikawa, T. Kaneyama, Y. Ohkura, Y. Kondo, and T. Isabell, Microsc. Anal. Nanotechnol. **24**, S9–S13 (2010).

[15] M. Haider, S. Uhlemann, E. Schwan, H. Rose, B. Kabius, and K. Urban, Nature **392**, 768 (1998).

[16] J. Iijima, Optik (Stuttgart) **48**, 193 (1977).

[17] J. O. Bovin, R. Wallenberg, and D. J. Smith, Nature **317**, 47 (1985).

[18] B. Gamm, H. Blank, R. Popescu, R. Schneider, A. Beyer, A. Gölzhäuser, and D. Gerthsen, Microsc. Microanal. **18**, 212 (2012).

[19] D. Alloyeau, B. Freitag, S. Dag, L. W. Wang, and C. Kisielowski, Phys. Rev. B **80**, 014114 (2009).

[20] C. O. Girit, J. C. Meyer, R. Erni, M. D. Rossell, C. Kisielowski, L. Yang, C.-H. Park, M. F. Crommie, M. L. Cohen, S. G. Louie, and A. Zettl, Science **323**, 1705 (2009).

[21] C. Kisielowski, Q. M. Ramasse, L. P. Hansen, M. Brorson, A. Carlsson, A. M. Molenbroek, H. Topsoe, and S. Helveg, Angew. Chem., Int. Ed. **49**, 2708 (2010).

[22] M. Fllueli, P. A. Buffat, and J. P. Borel, Surf. Sci. **202**, 343 (1988).

[23] M. Klimenkov, W. Matz, and J. v. Borany, Nucl. Instrum. Methods Phys. Res. B **168**, 367 (2000).

[24] W. J. Zhang and D. E. Miser, J. Nanopart. Res. **8**, 1027 (2006).

[25] P. Jensen, X. Blase, and P. Ordejón, Surf. Sci. **564**, 173 (2004).

[26] P. A. Stadelmann, Ultramicroscopy **21**, 131 (1987).

[27] J. Barthel and A. Thust, Ultramicroscopy **111**, 27 (2010).

[28] A. Weickenmeier and H. Kohl, Acta Crystallogr. **47**, 590 (1991).

[29] A. Rose, *Advances Electronics and Electron Physics* (Academic, New York, 1948).

[30] A. Thust, Phys. Rev. Lett. **102**, 220801 (2009).

[31] D. R. Lide, *CRC Handbook of Chemistry and Physics*, 79th ed. (CRC, Boca Raton, 1998), p. 5.13, 5.24.

[32] C. K. Acharya, D. I. Sullivan, and C. H. Turner, J. Phys. Chem. C **112**, 13607 (2008).

[33] Y. Mao, J. Yuan, and J. Zhong, J. Phys.: Conden. Matter **20**, 115209 (2008).

[34] M. l. Delalande, M. J. F. Guinel, L. F. Allard, A. Delattre, R. Le Bris, Y. Samson, P. Bayle-Guillemaud, and P. Reiss, J. Phys. Chem. C **116**, 6866 (2012).